TUDelft

Delft University of Technology

A deconvolution protocol of the mechanical relaxation spectrum to identify and quantify individual polymer feature contributions to self-healing

Montano, Vincenzo; Picken, Stephen J.; Van Der Zwaag, Sybrand; Garcia, Santiago J.

Important note
To cite this publication, please use the final published version (if applicable).
Please check the document version above.

PAPER

Check for updates

A deconvolution protocol of the mechanical relaxation spectrum to identify and quantify individual polymer feature contributions to self-healing

Vincenzo Montano, [ID] *[a] Stephen J. Picken,[b] Sybrand van der Zwaag[a] and Santiago J. Garcia [ID] [a]

Starting from experimental macro-rheological data, we develop a fitting protocol that succeeded in the separation of the overlapping relaxation phenomena in the dissipative regime for a set of intrinsic healing polymers healing most effectively near their glass transition temperature T_g. To allow for a proper deconvolution, the rheological master curves are converted to a relaxation spectrum ($H(\tau)$) and this is fitted using an optimized mechanical model, *e.g.* the Maxwell–Weichert model. The deconvolution of overlapping segmental mobility and reversible interactions is successfully demonstrated for a set of polyimide and polyamide polymers containing none, one and two reversible dynamic features near-T_g. Through the fitting parameters, the relaxation timescale of each feature and their apparent process enthalpies are obtained. The quantitative data obtained using the fitting protocol are then compared to macroscopic healing results. As a result, a clear correspondence between the energy stored by the system to accomplish reversible (*e.g.* H-bonds, $\pi-\pi$) and chain interdiffusion relaxation transitions and the healing efficiency of such polymers are obtained. The implementation of this protocol allows for a clearer identification of the relevant mechanisms in self-healing polymers and paves the way for the development of more efficiently healable polymeric systems.

1. Introduction

Intrinsic self-healing polymers can undergo multiple healing events, even at the same location, as the macromolecular design of these systems yields non-permanently consumed reversible chemical or physical bonds leading to the de-construction of crack interfaces brought in intimate contact.[1]

Supramolecular chemistry has been particularly beneficial for the development of intrinsic self-healing polymers, particularly at near room temperature.[2,3] Initial tack and short range interactions, followed by time-dependent long range chain interdiffusion and bond reformation, allow partial or full but in any case repeatable restoration of the original material properties,[4] such as mechanical,[5] barrier,[6] aesthetical or electrical properties.[7]

Many methods developed to identify the underlying physical molecular processes in polymer rheology in general and in self healing in particular have been described in the literature.[8–12]

Of the available methods, the analysis of frequency domain master curves used to probe polymer dynamics[9,10] should be regarded as a necessary first-order approximation to identify the polymer healing and kinetics.[11] The experimental tool that probes polymer dynamics over a wide range of frequencies is the well-known time–temperature superposition (TTS) principle.[13,14] Originally, TTS was developed for thermo-rheologically simple fluids but it is being used increasingly to analyse the behaviour of more complex and branched polymers.[15,16] Although self-healing polymers do not behave as simple fluids, the use of the TTS in self-healing polymers has revealed, amongst others, the existence of a clear correlation between terminal relaxation and the degree of substantial macroscopic healing.[12] Nevertheless, when multiple relaxations occur in a restricted timescale range (*i.e.*, overlapping phenomena), it is hard to precisely delineate the dissipation dynamics of the system with the approaches now in use. As a result, it is hard to identify the existence of concurrent and overlapping phenomena. This problem becomes relevant when analysing the frequency dependent viscoelastic domain of more advanced self-healing supramolecular polymers. In these systems, the dynamic nature of the network stickers often results in the dynamics of the transient network relaxation overlapping with dynamic phenomena occurring in the main chain (*i.e.* segmental mobility).

[a] *Novel Aerospace Materials Group, Faculty of Aerospace Engineering, Delft University of Technology, Kluyverweg 1, Delft, 2629 HS, The Netherlands. E-mail: v.montano@tudelft.nl*

[b] *Faculty of Applied Science, Delft University of Technology, Van der Maasweg 9, Delft, 2629 HZ, The Netherlands*

This journal is © the Owner Societies 2019

Phys. Chem. Chem. Phys., 2019, **21**, 10171–10184 | **10171**

In the literature, many reports demonstrate optimal intrinsic healing at temperatures close to T_g (glass transition) where the enhanced conformational mobility allows dynamic bond exchange and possibly macromolecular flow[6,17–19] without a substantial loss of mechanical properties. For such systems, the relaxation dynamics related to the presence of supramolecular stickers often overlaps with the main chain segmental mobility, resulting in misleading correlations between kinetics of macroscopic healing and the differences in the timescale of the relaxation processes as well as disagreements with the physical theories developed to theoretically explain intrinsic self-healing in polymers.[18–20] In that case, the macro-rheology does not show a clear separation between the two above-mentioned relaxation mechanisms or, in other terms, it is not possible to clearly distinguish a double plateau of the elastic component of the shear modulus $G'(\omega)$ in the analysed spectrum of frequency.[21] The effective overlap between molecular complexation/de-complexation of the reversible network and main chain segmental mobility is generally analysed by comparing macro-rheological data to molecular rheology predictions such as that proposed by Leibler, Rubinstein and Colby.[22] For systems showing overlap between main chain segmental mobility and reversible chain association, the analysis of particular features of the master curve, such as the slope of G' and G'' in the plateau region and the phenomenon of terminal relaxation, is used to prove compliance with the sticky reptation model, thereby proving the existence of reversible bonds.[18,23–25] More recently, new theories based on slip-link and double reptation models have aimed to elucidate the reason for the absence of the classical double 'Leibler' plateau in entangled systems bearing sticky units.[26,27]

Despite the elegance of the molecular rheology theories, the problem of defining the individual timescales of the overlapping relaxation phenomena related to stickers and segmental mobility remains unsolved and is addressed in this paper.

In a recent publication, Ankiewicz et al.[28] proposed the use of a continuous relaxation spectrum $H(\tau)$ to identify overlapping phenomena in complex polymers. For a series of model H-polymers, the relaxation spectrum $H(\tau)$ revealed relaxation peaks and timescales that could not be directly inferred from the frequency master curves. Following this work, Yesilyurt and co-workers[29] used an analogue mechanical model (the Maxwell–Weichert model) to determine the correct dissipation dynamics of five reversibly crosslinked hydrogels. The networks were formed from mixtures of two different phenylboronic acid derivatives having two unique diol complexation rates. In their work, the authors showed how the application of the mechanical model to the relaxation spectrum $H(\tau)$ allowed deconvolution of the relevant processes and separation of the contributions of the two complexation processes. Inspired by these two works, we introduce here a high resolution fitting protocol that enables the deconvolution of the overlapping dissipation dynamics attributed to main chain segmental mobility and reversible junction disengagement of reversible bonds through the use of mechanical analogous model fits, issuing a fundamental problem of near-T_g self-healing polymers where classical representation/analysis of

linear viscous data does not provide the distinction of multiple relaxation processes. The protocol yields a finite number of parameters that semi-quantitatively capture the different relaxation phenomena, providing an indirect measure of energy stored by each polymer feature during the single relaxation transition. To prove the concept, we used two unentangled polyamides and four near-T_g self-healing unentangled polyimides containing short aliphatic branches and aromatics responsible for π–π interactions.[18,25] The protocol presented here makes it possible to identify the individual contributions to healing showing a clear correspondence between the energy stored by the system to accomplish reversible (e.g. H-bonds, π–π) and chain inter-diffusion relaxation transitions and the healing efficiency of such polymers. The results of this study make it clear that it is important to have a certain temperature distance between T_g and the temperature for sticker relaxations to obtain the desired combination of significant mechanical healing and high mechanical properties. This quantified temperature distance can be used as a new design criterion for the synthesis of stronger yet efficient self-healing polymers.

2. Experimental and fitting protocols

2.1. Polymer synthesis

To evaluate the potential and validity of the protocol, a set of healable polyimide and polyamide polymers with a controlled polymer architecture, comparable molecular weights yet a different number of physical reversible groups (H-bonding and π–π interactions) were synthesized. A related non-healing linear polyamide was also synthesized.

Four self-healing polyimides (SH-PIs) were synthesized using the procedures described elsewhere.[18,19] The monomers used were three different aromatic dianhydrides, 4,4′-(4,4′-isopropylidenediphenoxy)bis(phthalic anhydride) (BPADA), 4,4′-oxydiphthalic anhydride (ODPA), and 4,4′-(hexafluotoiso-propylidene)diphthalic anhydride (6FDA), and a fatty dimer diamine derived from vegetable oil (Priamine 1075) (provided by Croda Nederland B.V.). The polyimides were divided into two Control Groups (Fig. 1). Control Group 1 consists of two polyimides obtained by polymerisation of Priamine and ODPA. The two polyimides differ in the stoichiometric molar feed of Priamine/ODPA: ODPA-p0.9 (with 10% mol excess of ODPA) and ODPA-p1.0 (at the theoretical stoichiometric ratio). Control Group 2 consists of three polyimides obtained by the polymerisation of Priamine and three distinct aromatic dianhydrides. The three polyimides differ in the degree of rotational freedom (DRF) of the anhydride rigid segment: BPADA-p1.0 (DRF = 2), ODPA-p1.0 (DRF = 1) and 6FDA-p1.0 (DRF = 0). DRF is related to the flexibility of the dianhydride moiety and in particular to the degree of rotational freedom around the central linker (e.g. the oxygen atom for ODPA-p1.0). A lower DRF implies a higher energy penalty to be paid to explore rotational states, as verified for this set of anhydrides both experimentally and through computations by Susa et al.[25]

A self-healing polyamide, C9PA, was synthesized using a one-step polymerisation process as described hereon. The monomers

10172 | Phys. Chem. Chem. Phys., 2019, **21**, 10171–10184

This journal is © the Owner Societies 2019
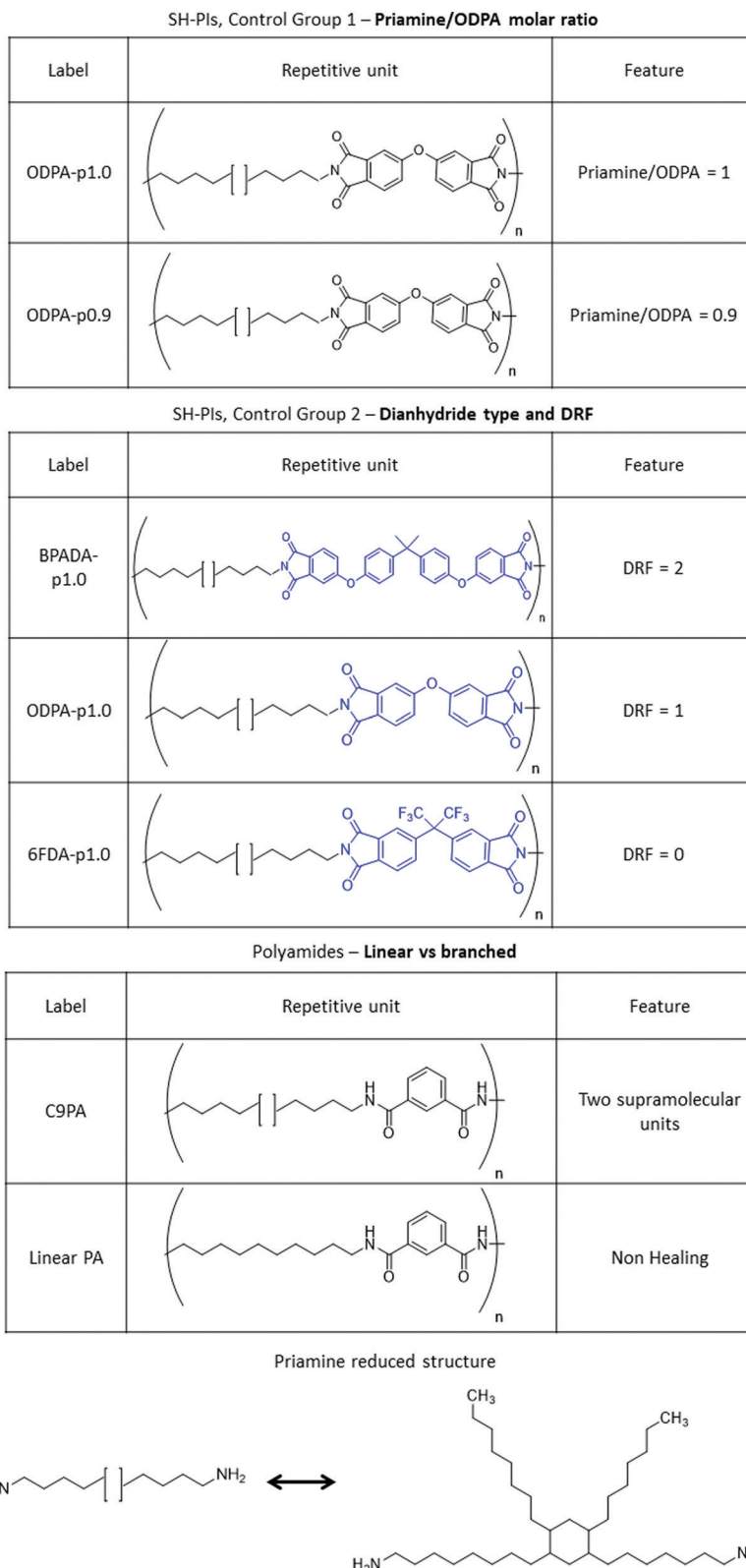
Fig. 1 Polymer classes investigated through the application of the Maxwell–Weichert mechanical analogue model. Priamine/ODPA is the molar ratio between the oil derivative dangling chain diamine monomer (Priamine 1075) and the rigid aromatic dianhydride (ODPA). DRF is the degrees of rotational freedom of the aromatic dianhydride block. At the bottom of this figure, we present the extended molecular structure of the branched moiety incorporated in ODPA-p0.9, ODPA-p1.0, 6FDA-p1.0, BPADA-p1.0, and C9PA polymers.

used were isophthaloyl chloride (IPC) (Sigma-Aldrich, purum, $\geq$98%) and Priamine 1075. The synthesis was conducted in 1-methyl-2-pyrrolidinone (NMP, Sigma-Aldrich, anhydrous, $\geq$99.5%) with a monomer molar concentration of 1 mmol mL^{-1}, using triethylamine (NEt3, Sigma-Aldrich, $\geq$99.5%) as an acid scavenger in a molar concentration of 1.2 mmol mL^{-1}. The molar monomer feed was set at a theoretical stoichiometric ratio.

IPC was recrystallized by sublimation as described elsewhere[30] and stored under nitrogen. Priamine was weighed directly in a three neck round bottom flask. 2/3 (vol) of the solvent (NMP) was added to the system. The mixture was magnetically stirred at 200 rpm to favour Priamine dissolution and purged under a nitrogen atmosphere. The solution was subsequently cooled to 0 °C using an ice bath in order to avoid unwanted side reactions between the diamine monomer (Priamine) and the acid scavenger (NEt3). NEt3 was then injected into the system using a syringe. IPC was weighed and dissolved in a separate flask in 1/3 (vol) of the reaction solvent (NMP). This solution was then injected into the main reactor using a syringe, keeping the system under vigorous magnetic stirring. The mixture was kept for 30 minutes at 0 °C. Ultimately, the temperature was increased to 55 °C for 3 hours. At the end of the reaction, the solution was left to cool down to room temperature. The viscous mixture was precipitated in an excess of demineralized water and washed three times. To favour the washing step, the precipitation was performed in a metal blade blender. The precipitate was sheared at 15 krpm for 1 minute. The polymer was separated from the mixture by using a vacuum conical flask and subsequently dried overnight under vacuum at 65 °C.

A related non-healing polyamide, Linear PA, was synthesized following an analogous procedure. The monomers used were IPC and 1,12-diaminodecane (Sigma-Aldrich, $\geq$98%). The synthesis was conducted in NMP with a monomer molar concentration of 1 mmol mL^{-1}, using NEt3 as an acid scavenger in a molar concentration of 1.2 mmol mL^{-1}. The molar monomer feed was set at the theoretical stoichiometric ratio.

2.2. Rheological measurements and tensile properties

Temperature sweep and frequency rheology tests were performed for all polymers to build the rheology master curves applying the time–temperature-superposition (TTS) principle. In all cases, a Haake Mars III rheometer (ThermoScientific) using the parallel plate geometry with a plate diameter of 8 mm was used. The data obtained at different temperatures were shifted using the Rheowin software routine (ThermoScientific). On the basis of preliminary strain amplitude sweep measurements, the shear strain amplitude was set at 0.1%. Temperature sweeps from 0 to 200 °C at a frequency of 1 Hz were performed to establish the shifting temperatures. Frequency sweep experiments from 10 to 0.1 Hz were performed with steps of ΔT = 5 °C over the temperature range from 0 to 80 °C for all polyimides and C9PA, while steps of ΔT = 10 °C were used for Linear PA in the range from 95 to 220 °C.

The maximum of the loss component of the shear modulus G'' in the temperature sweep tests was used as the internal reference to set the shifting temperature as it is at the midpoint of the dynamic phase transition. The reference shifting temperatures were $T_0^{\text{ODPA-p0.9}}$ = +20 °C, $T_0^{\text{ODPA-p1.0}}$ = +15 °C, $T_0^{\text{BPADA-p}}$ = +25 °C, and $T_0^{\text{6FDA-p}}$ = +30 °C.

C9PA and Linear-PA rheological master curves were built at the reference temperature of T_0^{C9PA} = +35 °C and $T_0^{\text{Linear PA}}$ = +120 °C.

Macroscopic healing was evaluated using tensile mechanical testing with dog-bone specimens according to the ASTM D1708 standard and applying a cross-head speed of 80 mm min^{-1}. To quantify the healing behaviour, pristine samples were cut with a sharp razor blade and directly put back in contact applying gentle pressure at ambient controlled temperature (21 °C). After placing the sample halves in contact in closely fitting moulds, the samples were subjected to healing treatments at specific healing temperatures for 11 days, without any additional load applied. The healing temperature was set at the temperature corresponding to the maximum of $\tan\delta$ ($\tan\delta = G''/G'$) extrapolated from preliminary temperature sweep analyses. All polymers exhibited intrinsic self-healing behaviour with the exception of Linear-PA. The lack of healing in Linear-PA is attributed to the high degree of main chain crystallisation induced by unperturbed hydrogen bonds among amide linkages as a result of the absence of aliphatic dangling chains (which are present in all other investigated systems).

2.3. Fitting protocol

The developed protocol is schematized in Fig. 2 and was set, validated and applied to the master curves of the 5 polymers as shown in Fig. 1. The construction of the rheology master curves is indicated as Step 0 in Fig. 2.

Step 1 consists of the determination of the best estimate for the continuous relaxation spectrum function $H(\tau)$exp. The spectrum $H(\tau)$exp. is derived from the experimental data of storage and loss moduli through the mathematical resolution of a well-known ill-posed problem.[13] The solution is attained by applying the non-linear regression method developed by Honerkamp and Weese,[31] as this method is both reliable and simple to use.[32] The source code of the algorithm can be found in the CPC Program library.[33] In this protocol, the minimum and maximum relaxation times are user-defined. In our case, we simply set $\tau_{\text{min}} = \dfrac{1}{\omega_{\text{max}}}$ and $\tau_{\text{max}} = \dfrac{1}{\omega_{\text{min}}}$, where ω_{max} and ω_{min} are the highest and the lowest angular frequency in the modulus data, as suggested in the library user manual.

The construction of $H(\ln\tau)$exp. facilitates the application of mechanical analogous modelling and sets up a multi-optimization problem, as shown in Steps 2 and 3.

Step 2 consists of the selection of the analogous mechanical model and the fit of the continuous relaxation spectrum $H(\tau)$exp. obtained in Step 1. Here, we selected the infinite Maxwell model (or the Maxwell–Weichert model) as the analogous mechanical model.

$$H_{\text{Model}}(\ln\tau) = \sum_{i=1}^{n} A_i \exp\left(-\frac{(\ln(\tau) - \ln(\tilde{\tau}_i))^2}{2\sigma_i^2}\right) \qquad (1)$$

The model entails an infinite number of Maxwell elements (a compliance and a dashpot in series) connected in parallel.

10174 | *Phys. Chem. Chem. Phys.*, 2019, **21**, 10171–10184

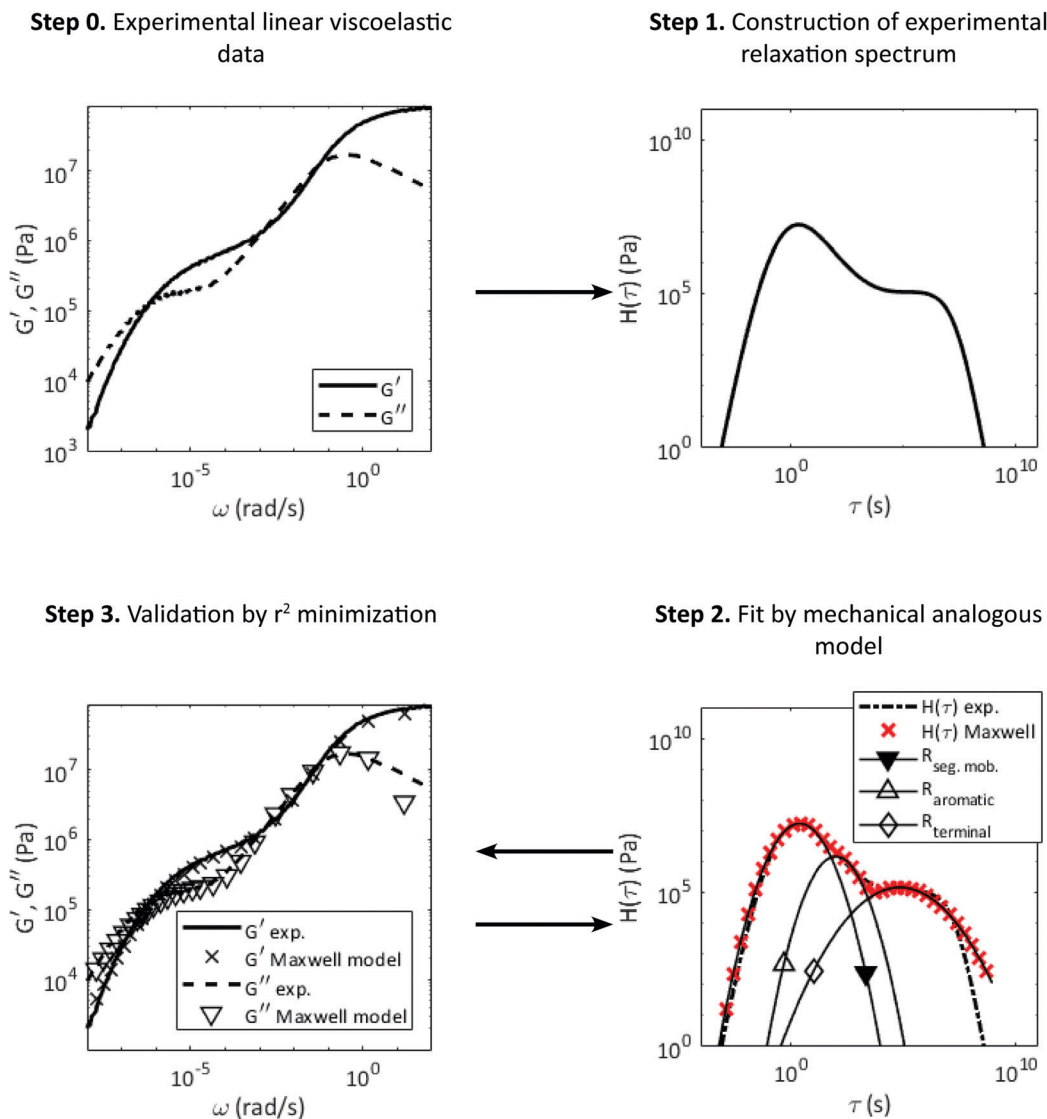This journal is © the Owner Societies 2019

Fig. 2   Fitting protocol to determine the number of dominant relaxations as applied to ODPA-p1.0: (i) experimental rheological master curve build up (Step 0); (ii) derivation of the relaxation spectrum $H(\tau)$ exp. (Step 1); (iii) construction of the fit function $H(\tau)$ Maxwell by using analogous mechanical models (Step 2); and (iv) validation and optimization of the mechanical model by reconstruction of the G' Maxwell model and G'' Maxwell model master curves (Steps 2 and 3).

The choice of this model allows us to approach the problem in the most general and unbiased way.

In eqn (1), $H_{\text{Model}}(\tau)$ is the model relaxation spectrum, $\ln(\tau)$ is the vector of time containing the experimental time extrapolated from $H(\tau)$ acquired in Step 1. $\tilde{\tau}$, A, and σ are fitting parameters. In particular, $\tilde{\tau}_i$ regulates the position on the time axis of a specific Maxwell element i, A_i controls the maximum magnitude, and σ_i controls the half height width.

The function H_{Model} must be validated with respect to two variables: the number of Maxwell elements $i \rightarrow i_{\text{optimum}}$ (a number that is *a priori* in principle unknown and which will determine the number of dominant relaxation mechanisms) and the set of fitting parameters ($\tilde{\tau}$, A, and σ).

The experimental $H(\tau)$exp. is fitted with a user-defined initial number of relaxation elements i, generating the fit function $H(\tau)$

Maxwell. The $H(\tau)$ Maxwell curve is represented by the red crosses in Step 2. Other markers in Step 2 represent the corresponding individual dominant relaxation mechanisms. Then, the optimal number of Maxwell elements and the set of best fitting parameter values are identified based on the minimization of the coefficient of determination (r^2) obtained by comparing the model storage and loss moduli (the G' Maxwell model and the G'' Maxwell model, reconstructed using the $H(\tau)$ Maxwell model) with the experimental moduli (G' exp. and G'' exp.), as shown in Step 3 and indicated with the arrows between Steps 2 and 3 as an iterative optimization process. The G' Maxwell model and the G'' Maxwell model are calculated using known relations[13] reported in eqn (2a) and (2b).

The optimization algorithm was set in Matlab R2017b using the lsqnonlin function to solve the nonlinear data fitting

This journal is © the Owner Societies 2019

Phys. Chem. Chem. Phys., 2019, **21**, 10171–10184 | **10175**

(MathWorks Inc.).

$$G'(\omega) = \int_{-\infty}^{\infty} \left[\frac{H(\ln \tau)\omega^2\tau^2}{1 + \omega^2\tau^2} \right] \mathrm{d} \ln \tau \qquad (2a)$$

$$G''(\omega) = \int_{-\infty}^{\infty} \left[\frac{H(\ln \tau)\omega\tau}{1 + \omega^2\tau^2} \right] \mathrm{d} \ln \tau \qquad (2b)$$

Baumgaertel and Winter[34] developed a conceptually similar procedure to infer the minimum number of Maxwell modes directly from $G^\star(\omega)$, which is implemented in the commercially available IRIS software package.

3. Results

The experimental frequency master curves of ODPA-p0.9, ODPA-p1.0, 6FDA-p1.0, BPADA-p1.0 and C9PA are presented in Fig. 4g–k. All polymers present the typical dynamical mechanical features of dynamic supramolecular networks.[3] For such systems, the molecular weight between effective interaction points (M_e) is lower than the minimum possible molecular weight for entanglements (Table 1 and ref. 18 and 25), so the apparent elastic plateau presence at intermediate frequency is attributed to the presence of supramolecular stickers, in accordance with the sticky reptation theory proposed by Rubinstein and Colby.[22] Such an apparent elastic plateau was also shown to exist in our previous work on self-healing polyimides similar to the ones used in this work.[25] None of these master curves show any clear separation between the relaxation phenomena associated with main chain segmental mobility and those with the supramolecular bonds.

The fitting protocol shown in Section 2.3 was applied to all rheological data sets for the 6 polymers explored.

Table 2 shows the r^2 values obtained during the fitting process to establish the optimal number of relaxation mechanisms i. Three relaxation phenomena ($i_{\text{optimum}} = 3$) were identified for the SH-PIs (ODPA-p0.9, ODPA-p1.0, 6FDA-p1.0, and BPADA-p1.0), four in the case of the self-healing polyamide C9PA with aromatics and H-bonds ($i_{\text{optimum}} = 4$) and another three for the non-healing Linear PA ($i_{\text{optimum}} = 3$).

Fig. 3a–f show for each polymer the optimal fit function with its corresponding reconstructed $H(\tau)$ Maxwell in red crosses, while Fig. 4g–l show the validation curves comparing the

Table 2 Coefficient of determination (r^2) obtained when comparing the experimental master curve with the reconstructed master curve after the fitting process. "i" indicates the number of Maxwell elements used in the fitting protocol. The optimum number of relaxation mechanisms for each polymer (*i.e.* Maxwell elements in series) is highlighted in bold and italic

	$i = 1$	$i = 2$	$i = 3$	$i = 4$	$i = 5$
ODPA-p0.9					
$r^2[G'(\omega)]$	0.3421	0.8406	*0.8496*	0.8430	0.6297
$r^2[G''(\omega)]$	—	—	—	—	—
ODPA-p1.0					
$r^2[G'(\omega)]$	0.9355	0.9479	*0.9566*	0.9549	0.9541
$r^2[G''(\omega)]$	0.9162	0.9134	*0.9176*	0.9129	0.9118
6FDA-p1.0					
$r^2[G'(\omega)]$	0.9060	0.9220	*0.9350*	0.9322	0.9339
$r^2[G''(\omega)]$	0.6311	0.6449	*0.6498*	0.6474	0.6441
BPADA-p1.0					
$r^2[G'(\omega)]$	0.9531	0.9722	*0.9860*	0.9853	0.9852
$r^2[G''(\omega)]$	0.8901	0.8963	*0.8975*	0.8957	0.9118
	$i = 2$	$i = 3$	$i = 4$	$i = 5$	$i = 6$
PADI					
$r^2[G'(\omega)]$	0.9095	0.9100	*0.9124*	0.9110	0.8876
$r^2[G''(\omega)]$	0.8139	0.8041	*0.8142*	0.8091	0.3648

experimental and the reconstructed master curves. It should be noted that all inferred relaxation peaks (both experimental and model) fall in the range of validity proposed by Davies and Anderssen[35] and extensively verified by McDougall *et al.*[32] for the method developed by Weese and Honerkamp to construct the continuous relaxation spectrum using the mathematical operations described above. According to the Davies and Anderssen sampling localisation,[35] the reliable interval for a truly valid relaxation time τ is $\tau_{\text{min}} = \dfrac{e^{\pi/2}}{\omega_{\text{max}}}$; $\tau_{\text{max}} = \dfrac{e^{-\pi/2}}{\omega_{\text{min}}}$, which are marked by sets of two dashed vertical lines in Fig. 3a–f.

The validation results in Fig. 4g–k show that the protocol captured the entire relaxation of the frequency set for the self-healing polymers. The sets of fitting parameters regulating time position ($\tilde{\tau}$), magnitude (A) and width (σ) of the individual relaxations for each polymer are reported in Table 3. Two overlapping phenomena at intermediate relaxation times were found for the set of SH-PIs while three overlapping relaxation mechanisms were identified for SH-PA. In the case of the high T_g non-healing system (Linear PA), the protocol identified two overlapping relaxations at intermediate times, as for the SH-PIs.

As will be shown in the Discussion section, each of the identified individual relaxation phenomena can be attributed to a specific polymer architectural feature having a specific effect on the viscoelastic relaxation profile, namely segmental mobility, aromatic interactions, H-bonds and terminal relaxation.

4. Discussion

4.1. Type and distribution of relaxation events

The fitting protocol applied to the experimental relaxation spectrum clearly reveals the existence of different relaxation

Table 1 Selected polymer properties: molecular weight distribution (M_w, Đ), apparent molecular weight between entanglements ($M_{e,app}$) as calculated using rubber elasticity ($M_e = \rho R T_0 / G_N$, where ρ is the material density, R is the universal gas constant, T is the shifting temperature and G_N is the plateau modulus as obtained from the van Gurp–Palmen plot), and T_g as obtained by DSC analysis. Linear-PA molecular weight distribution is not available since this polymer is not soluble in the available GPC solvents

Polymer	M_w (kDa)	Đ	$M_{e,app}$ (kDa)	DSC T_g (°C)
ODPA-p1.0	32	2.0	2.9	13
ODPA-p0.9	32	2.0	2.1	17
BPADA-p1.0	29	1.6	3.3	24
6FDA-p1.0	41	2.0	3.3	25
C9PA	17	1.9	4.6	25
Linear-PA	n.a.	n.a.	0.9	120

10176 | *Phys. Chem. Chem. Phys.*, 2019, **21**, 10171–10184
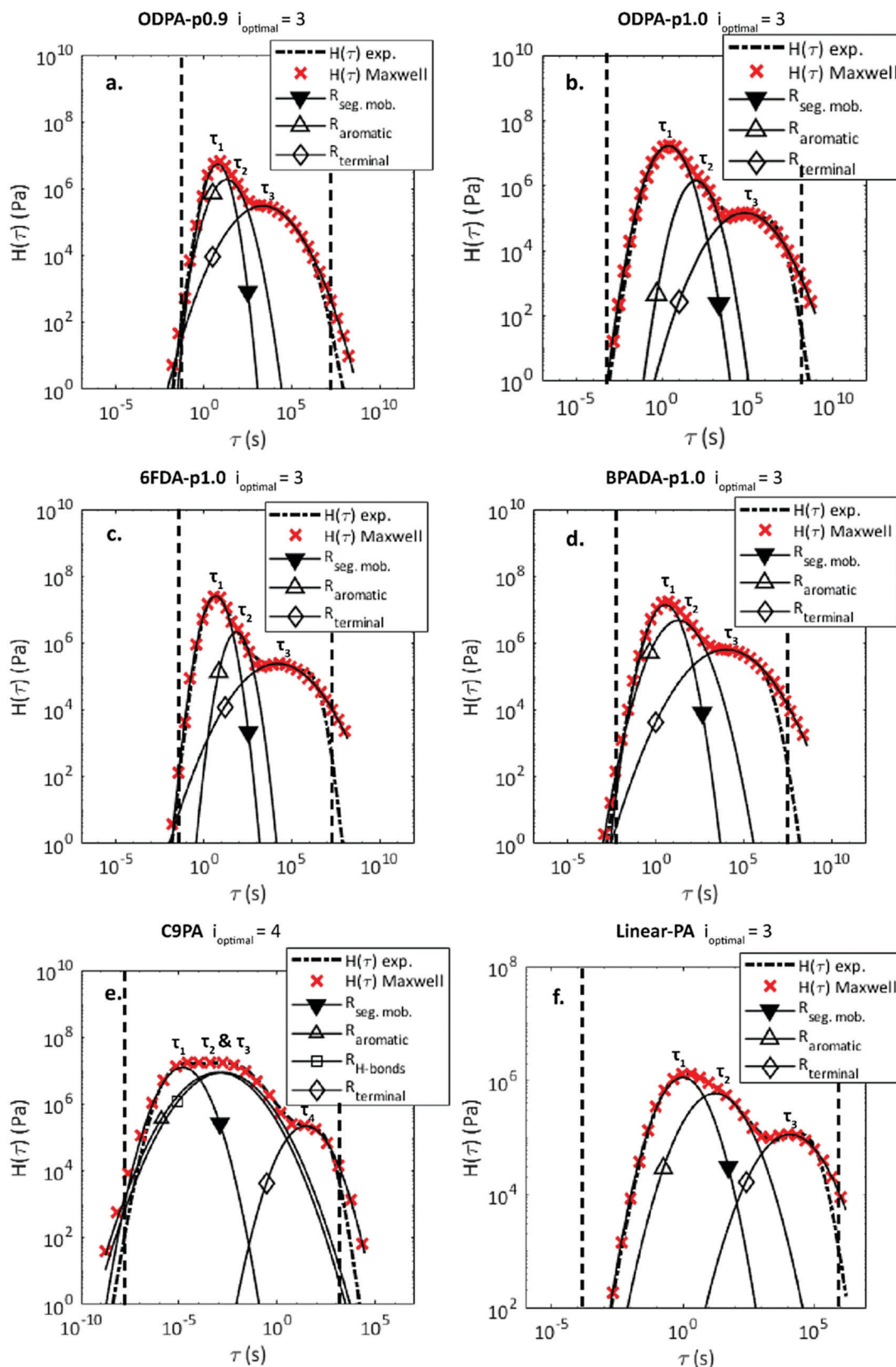
This journal is © the Owner Societies 2019

Fig. 3 Fitting results and validation after protocol implementation. (a–f) Optimal fit function $H(\tau)$ Maxwell (red ×) and dominant relaxation mechanism (line with markers) on top of experimentally calculated relaxation spectrum $H(\tau)$ exp. (−●−●−). The individual relaxations can be related to the presence of certain polymer features as discussed in the Discussion section and shown here with different markers (segmental relaxation $R_{seg. mob.}$ in ▼, aromatic interaction $R_{aromatic}$ in Δ, hydrogen bond interaction $R_{H-bonds}$ in □, and terminal relaxation $R_{terminal}$ in ◊). Vertical dash lines show the lower and upper limits of validity of relaxation times for the continuous relaxation spectrum as inferred by Davies et al.[35]
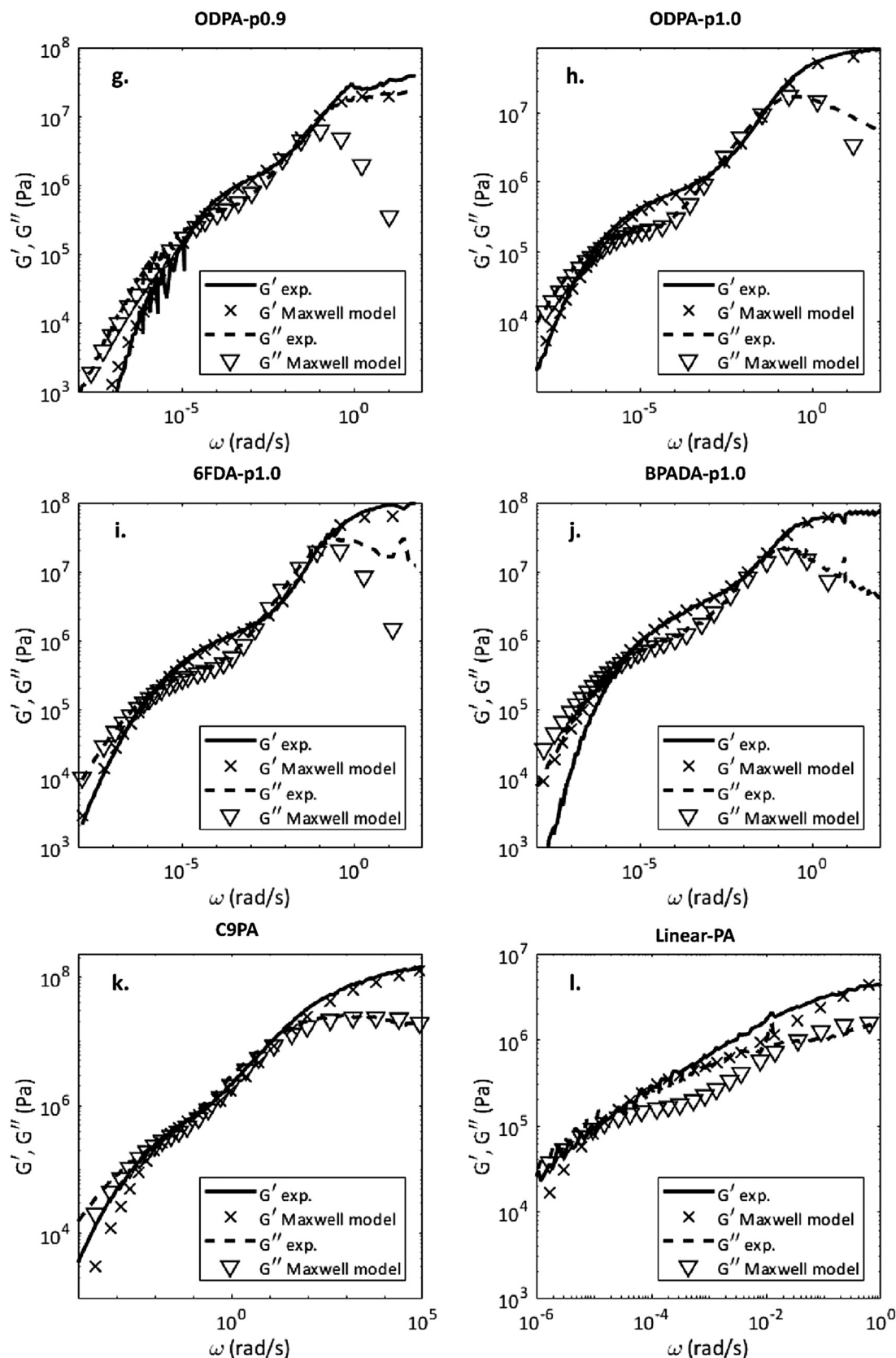
Fig. 4 (g–l) Comparison of the experimental moduli G' exp. and G'' exp. (continuous and dashed lines) and the moduli derived from the fitting procedure G' Maxwell model and the G'' Maxwell model ($\times$ and $\triangledown$), showing good correlation.

Table 3 Fitting parameters as output by protocol application to the set of SH-PIs, the self-healing polyamide (C9PA) and high T_g non-healing polyamide (Linear-PA)

Polymer	$\tilde{\tau}_1$ (s)	$\tilde{\tau}_2$ (s)	$\tilde{\tau}_3$ (s)	$\tilde{\tau}_4$ (s)	A_1 (MPa)	A_2 (MPa)	A_3 (MPa)	A_4 (MPa)	σ_1 (—)	σ_2 (—)	σ_3 (—)	σ_4 (—)
ODPA-p0.9	6.09	19.8	2.22×10^3	—	5.47	1.89	0.306	—	1.06	0.747	0.403	—
ODPA-p1.0	2.46	100	7.08×10^4	—	17.2	1.47	0.146	—	0.699	0.758	0.401	—
6FDA-p1.0	4.74	70.0	1.56×10^4	—	25.5	2.16	0.241	—	1.02	1.03	0.350	—
BPADA-p1.0	3.42	18.9	1.00×10^4	—	14.0	4.73	0.638	—	0.796	0.562	0.343	—
C9PA	1.5×10^{-5}	1.0×10^{-3}	1.7×10^{-3}	31.18	12.6	8.90	8.90	0.231	0.639	0.379	0.379	0.675
Linear-PA	1.00	16.8	1.22×10^4	—	1.14	0.596	0.112	—	0.676	0.543	0.505	—

mechanisms (Fig. 3a–f) as it shows the presence of overlapping relaxations not identifiable in simple experimental frequency master curves. The identification of all the relaxations taking place allows discussing the contribution of different polymer features to a given macroscopic phenomenon, *e.g.* self-healing, in a relatively simple approach in the case where the polymer architecture is known.

ODPA-p1.0 is a polyimide showing complete macroscopic healing in a three stage process consisting of fast-tack followed by time dependent long range interactions (self-diffusion) at the temperature of interest used in this work.[18] For this polymer, the fitting protocol shows three relaxation mechanisms (Fig. 3b). Two of these phenomena strongly overlap at short-intermediate timescales ($\tilde{\tau}_1$ and $\tilde{\tau}_2$) in the so-called transition region. A third relaxation mechanism is identified for long timescales ($\tilde{\tau}_3$) in the so-called terminal region. This branched unentangled low molecular weight polymer owes its high mechanical properties below T_g to the presence of non-covalent π–π interactions in the hard blocks and, to a lesser extent, to side branch interactions in the soft blocks (see the molecular architecture in Fig. 1 and ref. 19) as has been demonstrated by combining rheology and NMR techniques.[25] In a near-T_g healing polymer such as ODPA-p1.0, with a known and relatively simple polymer architecture, it is possible to allocate the transition region relaxations ($\tilde{\tau}_1$ and $\tilde{\tau}_2$) to short range main chain segmental mobility and to the opening of a transient network constituted by physical reversible interactions among dianhydride aromatic units. Here, $\tilde{\tau}_1$ is attributed to the main chain segmental mobility as this relaxation phenomenon at such short time scales requires low energetic main chain conformation rearrangements incompatible with physical crosslinks. It follows that $\tilde{\tau}_2$ can be associated with the aromatic interaction disjunction. Ultimately, since ODPA-p1.0 is a non-crosslinked polymer, the terminal relaxation ($\tilde{\tau}_3$) is associated with sticky chain reptation, when the chain is able to escape its 'tube'.[25] In analogy to our analysis of ODPA-p1.0, the three relaxation events observed in the other polymers with comparable architecture, namely ODPA-p0.9 (Fig. 3a), 6FDA-p1.0 (Fig. 3c), and BPADA-p1.0 (Fig. 3d), can be associated with main chain segmental mobility ($\tilde{\tau}_1$), physical network dissociation given by aromatic interactions ($\tilde{\tau}_2$), and chain reptation ($\tilde{\tau}_3$).

The results and analysis are somewhat different for the case of the polymer including an extra polymer feature (H-bonding), namely C9PA. In this case, the optimum number of relaxation events is four ($i_{optimum} = 4$), as shown in Fig. 3e and confirmed by the high values of r^2 as presented in Table 2. For this polymer, a broad transition region with a higher relaxation

strength (absolute value of $H(\tau)$) at short-intermediate timescales can be observed. The optimized fitting reveals three deconvoluted relaxation events ($\tilde{\tau}_1$, $\tilde{\tau}_2$, and $\tilde{\tau}_3$) in the broad transition region present at short-intermediate timescales, although it should be noted that two of these strongly overlap in the time domain ($\tilde{\tau}_2$ and $\tilde{\tau}_3$), possibly suggesting that these relaxation mechanisms cooperatively contribute to one dominant dynamic process. Based on the molecular design and on the optimisation of the dominant relaxation mechanisms using the protocol ($i_{optimum} = 4$), the relaxations can be attributed to the overlap of main chain segmental mobility ($\tilde{\tau}_1$) and the disengagement of a double transient network constituted by hydrogen bonds between the amide units and those between the aromatics ($\tilde{\tau}_2$ and $\tilde{\tau}_3$). The strong overlap of these two suggests that these phenomena are strongly bound to each other, which is not surprising considering the proximity of the two responsible segments in the polymer architecture (Fig. 1). $\tilde{\tau}_4$ at long timescales is attributed to terminal relaxation.

4.2. Physical meaning of the fitting parameters

The relaxation spectrum $H(\tau)$ has the nature of a distribution function, even though it has the dimension of a modulus rather than the dimensionless character of a common distribution function. Strictly speaking, h is defined as: $h = H/G_g$, where G_g is the stress/strain ratio for an instantaneous deformation.[13] Considering $\tau^\star$ as a generic relaxation time, the absolute value of the relaxation spectrum $|H(\tau^\star)|$ is proportional to the energy dissipation at that time location. For this reason, the area under the distribution curve $H(\tau)$ is proportional to the energy stored during the relaxation process and therefore to the plateau of G' obtained *via* macro-rheology. Hence, a physical meaning can be bestowed onto the fitting parameters obtained. In particular, for a certain relaxation mechanism i, $\tilde{\tau}_i$ defines the relaxation time corresponding to the maximum of dissipation, so it regulates the kinetics of the relaxation transition. The ratio A_i/σ_i represents the area under the curve of the individual relaxation event and is therefore related to the energy stored in the system related to the relaxation transition i and is proportional to G_g (stress/strain ratio for an instantaneous deformation). We will refer to the ratio A_i/σ_i as an "energy distribution shape" parameter. In this manner, we can correlate the macroscopic healing behaviour to quantifiable data extracted from the fitting protocol.

In self-healing polymers, a precise indication of supramolecular bond lifetime (τ_b) is fundamental to understand the timescale of the interfacial wetting step of the healing process.[11] For the set of

This journal is © the Owner Societies 2019

Phys. Chem. Chem. Phys., 2019, **21**, 10171–10184 | 10179

SH-PIs, $\tilde{\tau}_2$ was associated with the opening of a transient network consisting of aromatic interactions. The $\tilde{\tau}_2$ results obtained by the protocol implementation (Table 3) are consistent with the

intermediate range of bond lifetime ($1 < \tau_b < 100$ s) previously reported for functional (and self-healing) supramolecular polymers.[36,37] This confirms the hypothesis of the existence of a short-term healing step consisting of interfacial wetting, followed by a long-term chain interdiffusion and randomization related to terminal flow originally proposed by Wool and co-workers.[38]

The broadening of the transition region in C9PA when compared to the analysed SH-PIs can be evaluated quantitatively by analysing the difference in the ratio of the fitting parameters A_2/σ_2 shown in the summary table, Table 4. The increase in the value of A_2/σ_2 can be attributed to the additional amount of dissipated energy necessary to open up the double

Table 4 Ratio of the fitting parameters A_i/σ_i for SH–PIs and SH–PA output obtained by using the protocol. The ratio A_i/σ_i is proportional to G_g and so it is related to the energy stored by the system to accomplish each relaxation transition

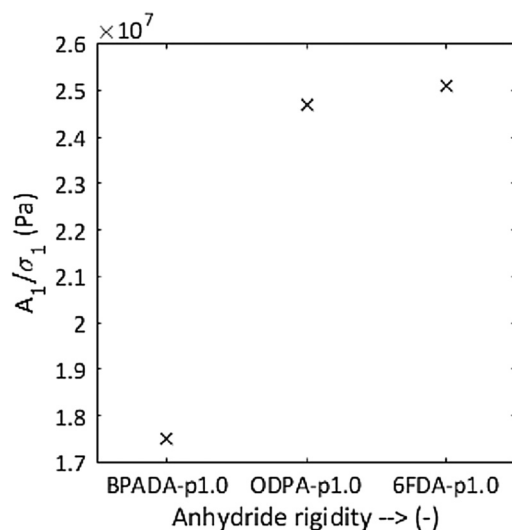| Relaxation mechanisms	$i_{optimal}$	Polymer	A_1/σ_1 (MPa)	A_2/σ_2 (MPa)	A_3/σ_3 (MPa)	A_4/σ_4 (MPa)
• Segmental mobility	3	ODPA-p0.9	5.16	2.53	0.76	—
• Aromatics		ODPA-p1.0	24.6	1.94	0.36	—
• Terminal relaxation		6FDA-p1.0	25	2.09	0.69	—
		BPADA-p1.0	17.59	8.41	1.86	—
• Segmental mobility	4	C9PA	19.72	23.48	23.48	0.34
•Aromatics						
•H-bonds						
•Terminal relaxation						

Fig. 5 Maxwell–Weichert model best fit of energy distribution shape related to main chain segmental mobility (A_1/σ_1) for SH–PIs in Control Group 2 with increasing main chain rigidity. A higher energy stored by the system to accomplish the relaxation transition corresponds to a higher main chain rigidity.
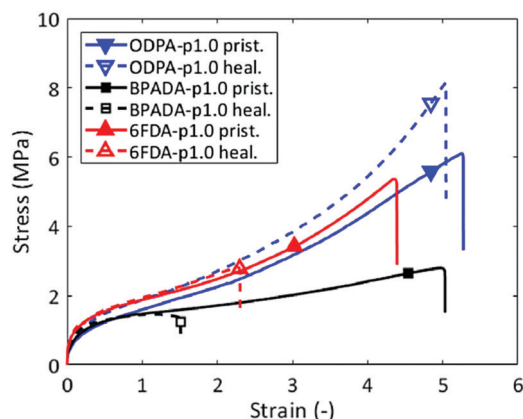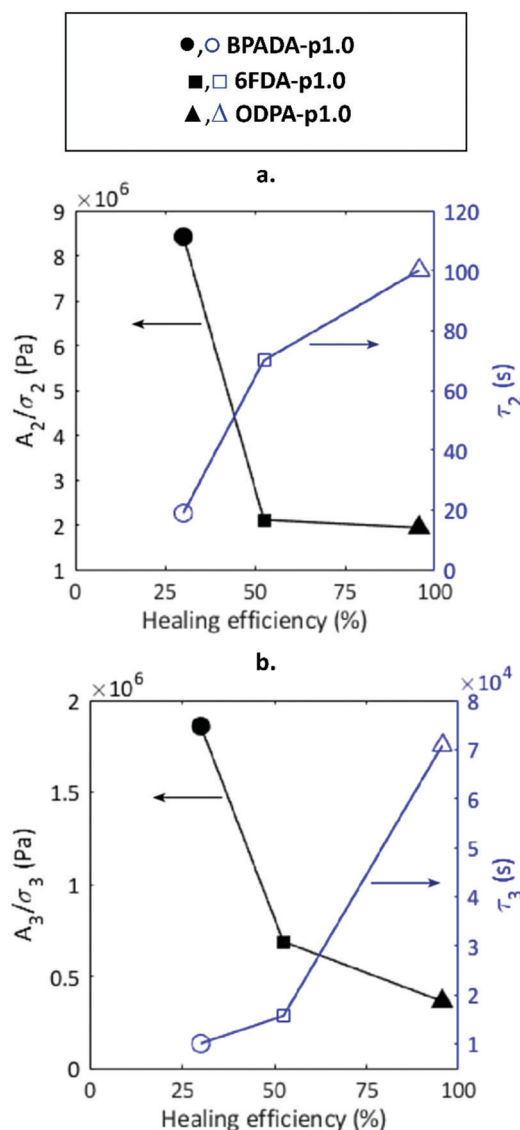

Fig. 6 Mechanical tensile testing of pristine and healed PI Control Group 2 after 11 days at $T_{healing} = T_g$.

Fig. 7 Energy distribution shape (A/σ) and relaxation time constant (τ) as obtained for SH–PIs in Control Group 2 and related long term (11 days) healing efficiency. (a) Parameters related to reversible interactions among aromatics (A_2/σ_2, τ_2). (b) Parameters related to the chain interdiffusion transition (A_3/σ_3, τ_3).

10180 | *Phys. Chem. Chem. Phys.*, 2019, **21**, 10171–10184

This journal is © the Owner Societies 2019

transient network (or stronger physical crosslinks due to the presence of two supramolecular features).

Similarly, the ratio A_1/σ_1 can be related to the main chain rigidity. This transition is attributed to the main chain segmental mobility. So, for polymers with a higher main chain flexibility, we reasonably expect a lower amount of energy stored by the system to accomplish the relaxation. Considering the series of SH-PIs, Control Group 2, the highest chain flexibility of BPADA-p1.0 (DRF = 2) is linked to the lowest stored energy A_1/σ_1 (Table 4 and Fig. 5). Analogously, the higher chain flexibility of ODPA-p1.0 (DRF = 1) when compared to

6FDA-p1.0 (DRF = 0) results in a relatively lower A_1/σ_1 (Table 4 and Fig. 5).

So, fundamental arguments along with experimental evidence seem to confirm the physical meaning assigned to the optimized fitting parameters.

4.3. Relating fitting protocol outcomes to self-healing efficiency

Theoretical studies by Wool and co-authors[38,39] demonstrated that in non-crosslinked polymers, crack-healing consists of five steps: segmental surface rearrangements, surface approach,
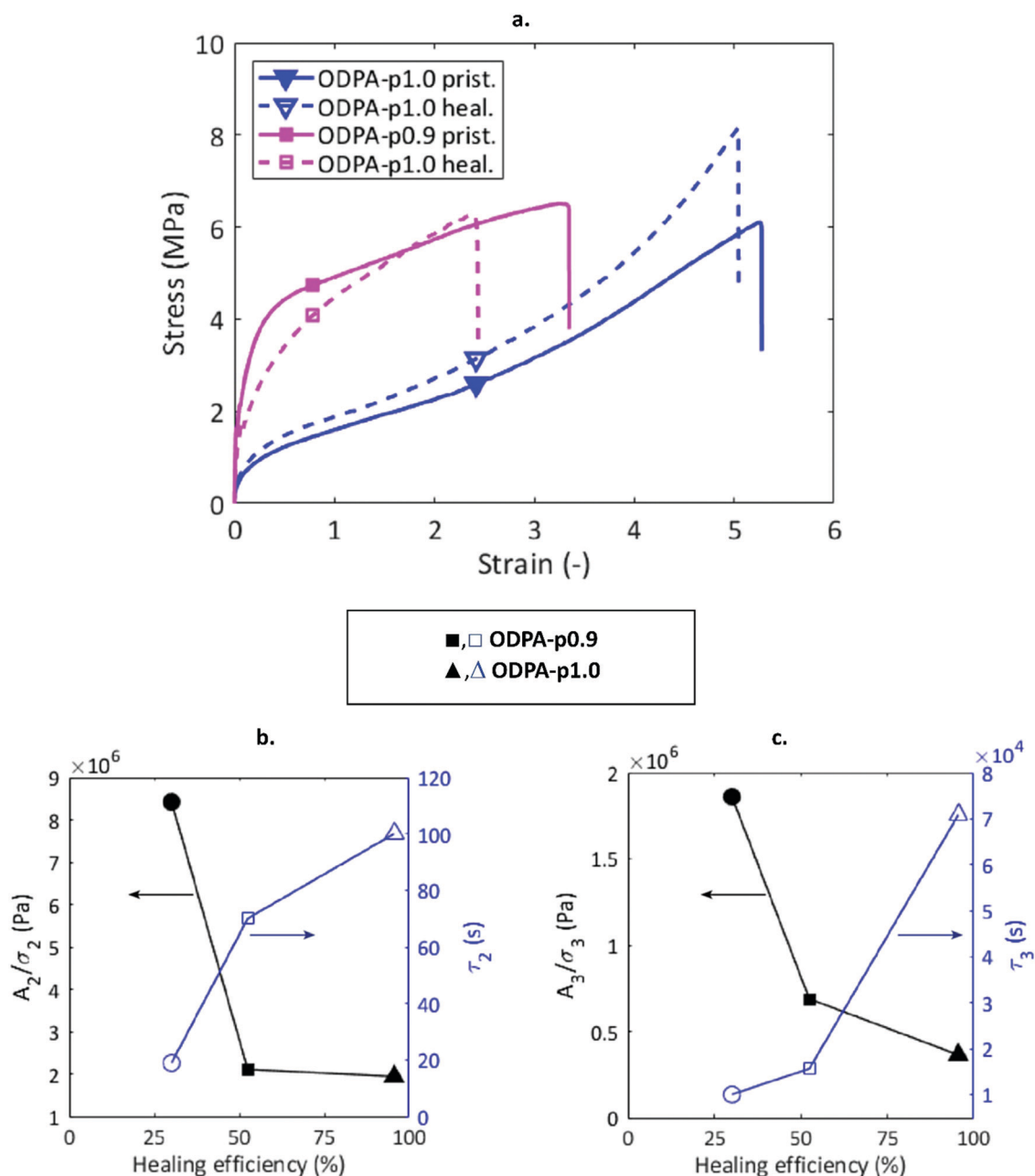

Fig. 8 (a) Mechanical tensile testing of pristine and healed PI Control Group 1 after 11 days at $T_{healing} = T_g$. (b and c) Energy distribution shape and relaxation time constants as obtained for Control Group 1. (b) Parameters related to reversible interactions among aromatics (A_2/σ_2, τ_2). (c) Parameters related to the chain interdiffusion transition (A_3/σ_3, τ_3).

wetting, diffusion, and randomization. The reptation model theory semi-quantifies such healing events and shows that the recovery of the fracture stress is related to molecular weight M and time t via $\sigma \propto (t/M)^{1/4}$. While this dependence on time and molecular weight was experimentally shown for crack healing poly(methylmethacrylate) (PMMA) and supramolecular elastomers,[40] it is not reflected in the series of SH-PIs, as has been reported elsewhere.[19,25] Using healing efficiency (HE) as

$$HE = \frac{\varepsilon_{b,healed}}{\varepsilon_{b,pristine}}$$ with ε_b being strain at break as an indicator for

healing efficiency, there is no real correlation between the number molecular weight (M_n) shown in Table 1 ($M_{n,ODPA-p} < M_{n,BPADA-p} < M_{n,6FDA-p}$) and the experimental long term healing data extrapolated by tensile mechanical data shown in Fig. 6 ($HE_{BPADA-p} < HE_{6FDA-p} < HE_{ODPA-p}$) nor with the terminal

relaxation values obtained from the macro-rheology tests where shorter timescales are obtained for BPADA-p1.0 compared to 6FDA-p1.0 and ODPA-p1.0.[19]

Interestingly, the analysis of the fitting protocol relaxation time ($\tilde{\tau}_i$) from Table 3 gives similarly contradicting results. As shown in Fig. 7a and b (open markers), low values of healing efficiency correspond to the shorter timescales of the BPADA-p1.0 polymer (low values of τ_2 and τ_3), while high healing efficiency corresponds to the longer timescales of 6FDA-p1.0 and ODPA-p1.0.

The weak agreement between theory, macro-rheology and long term healing experiments can be accounted for by the fact that the reptation model proposed by Wool does not consider bond cleavage and intermolecular interactions. We argue that this information can be inferred by the analysis of the energy
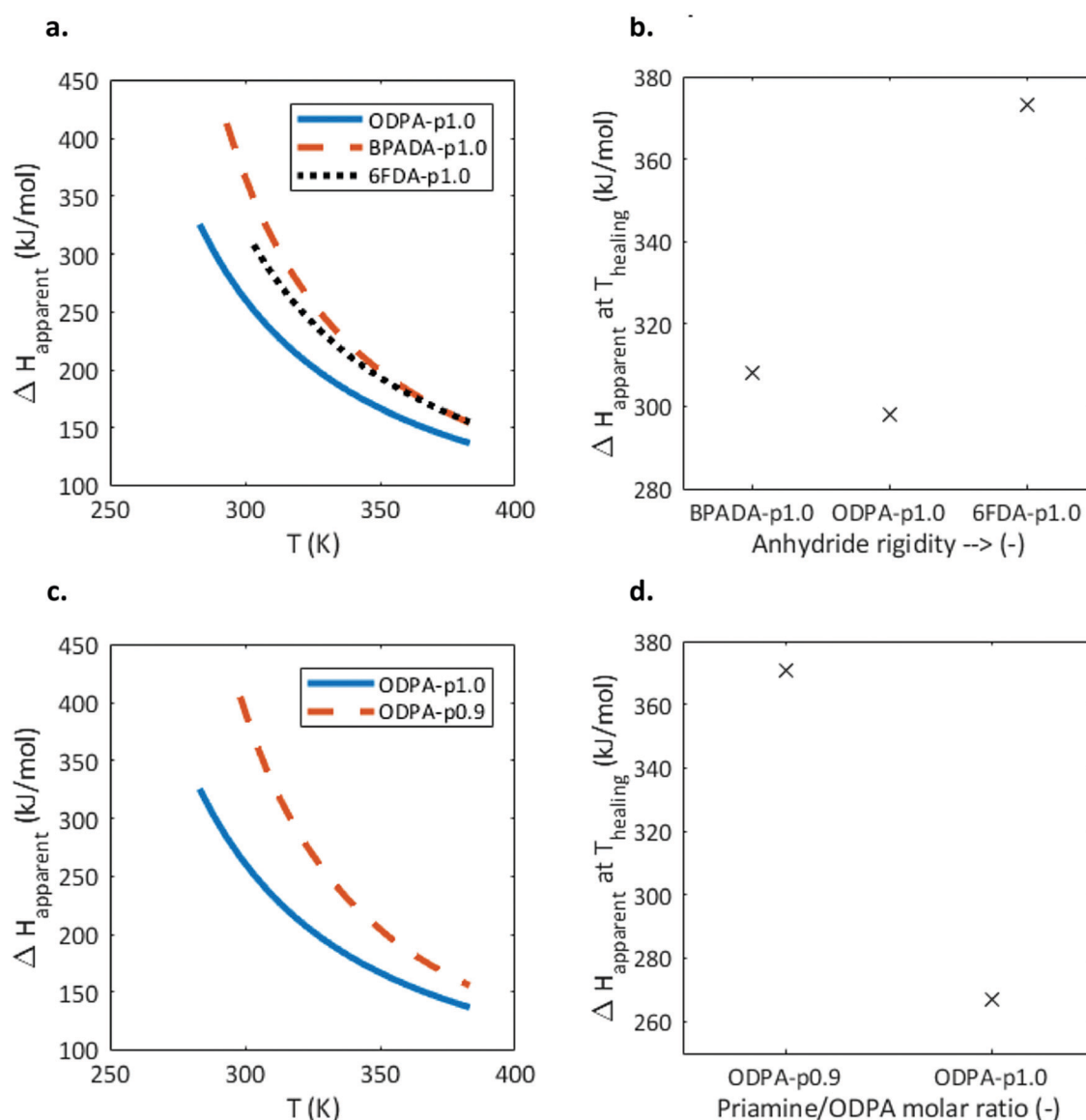

Fig. 9 Apparent enthalpy of relaxation transition computed through the WLF fit of experimental rheology frequency master curves. (a and b) Effect of the dianhydride type. (c and d) Effect of the ODPA/Priamine molar ratio. The enthalpy barrier increases with higher degrees of rotational freedom and with a lower amount of branched diamine, acting as a limiting factor on the long term healing behaviour of the SH-PEIs.

10182 | *Phys. Chem. Chem. Phys.*, 2019, **21**, 10171–10184

This journal is © the Owner Societies 2019

distribution shape parameter (A/σ). As discussed in Section 4.2, the energy distribution shape parameter (A/σ) reflects the energy that the system stores during the relaxation transition. Therefore, in our analysis, the ratio A_2/σ_2 is attributed to the energy needed to break the reversible interactions among aromatics and A_3/σ_3 is attributed to the energy needed for chain interdiffusion. If bond cleavage and intermolecular interactions play a major role in determining a high healing efficiency, then low A/σ values should yield a high healing efficiency. In other words, less energy must be stored by the system to relax and self-heal. In effect, as shown in Fig. 7b (filled markers), we indeed found this correspondence: lower A_2/σ_2 and A_3/σ_3 values belong to high healing efficiency polymers.

An independent estimation of the energy stored by the system in the overall relaxation process can be obtained using the William–Landel–Ferry fit to the experimental rheological shift factors.[13] The results of the calculation are shown in Fig. 9a and b. For the spectrum of shifted temperatures, $H_{apparent}$ follows the trend of the energy values obtained from the fitting as shown in Fig. 7 and healing efficiency.

Similar considerations can be made when comparing two PIs with different branched monomer/aromatic dianhydride (Priamine/ODPA) ratios. In these polymers, there is also no agreement between macroscopic healing efficiency, macro-rheology and fitting protocol relaxation time ($\tilde{\tau}_i$ trend represented in Fig. 8b). However, the trend of A_3/σ_3 (Fig. 8c) and $\Delta H_{apparent}$ of the overall relaxation process computed through the WLF fit of the shifted data (Fig. 9c and d) is in mutual agreement and in accordance with the macroscopic healing data reported in Fig. 8a.

In conclusion, while high chain flexibility and fast relaxation time constants seem to govern the first stage of self-healing (interfacial healing),[41] we show for the first time in a quantitative manner for a number of polymers that the energy stored by the system during the healing process is crucial when considering the design of efficient self-healing polymers because it regulates reversible bond cleavage and chain interdiffusion. The fitting protocol developed offers a simple way of identifying individual relaxation contributions and estimating the energetic contribution to the involved relaxation processes.

5. Final remarks

We successfully developed and implemented a deconvolution protocol involving the conventional macro-rheology master curve. This approach enables the determination of the number of individual relaxations related to different polymer features contributing to the overall relaxation spectrum, showing for the first time a clear separation between the relaxation timescales associated with main-chain segmental mobility and reversible lateral interactions in near-T_g polymers. The concept was proven for a set of self-healing polyimides (SH-PIs), a self-healing polyamide (C9PA) and a non-healing reference polyamide (Linear PA). For these polymers, the protocol accurately identified the overlapping

relaxation dynamics attributed to main chain segmental mobility and a number of supramolecular interactions as well as the terminal relaxation. The continuous relaxation spectrum unveiled some features that could not have been inferred from classical representations of linear viscoelastic data.

The approach bridges an existent gap between the macro-rheological analysis based on relaxation timescales and the macroscopic healing data and opens the way to predicting the long term macroscopic healing behaviour as a function of the polymer architecture. With the method presented here, we can identify the effect of the implementation of a number of reversible chemistries on the rheological relaxation mechanics and therefore on the healing behaviour. This should allow a more meaningful and more effective design of self-healing polymers.

Conflicts of interest

There are no conflicts to declare.

Acknowledgements

References

1 M. D. Hager, P. Greil, C. Leyens, S. van der Zwaag and U. S. Schubert, *Self-healing materials*, 2010, vol. 22.

2 P. Cordier, F. Tournilhac, C. Soulié-Ziakovic and L. Leibler, Self-healing and thermoreversible rubber from supramolecular assembly, *Nature*, 2008, **451**, 977–980.

3 F. Herbst, S. Seiffert and W. H. Binder, Dynamic supramolecular poly(isobutylene)s for self-healing materials, *Polym. Chem.*, 2012, **3**, 3084.

4 S. D. Bergman and F. Wudl, Mendable polymers, *J. Mater. Chem.*, 2008, **18**, 41–62.

5 W. Post, A. Cohades, V. Michaud, S. van der Zwaag and S. J. Garcia, Healing of a glass fibre reinforced composite with a disulphide containing organic-inorganic epoxy matrix, *Compos. Sci. Technol.*, 2017, **152**, 85–93.

6 S. Bode, L. Zedler, F. H. Schacher, B. Dietzek, M. Schmitt, J. Popp, M. D. Hager and U. S. Schubert, Self-healing polymer coatings based on crosslinked metallosupramolecular copolymers, *Adv. Mater.*, 2013, **25**, 1634–1638.

7 S. J. Benight, C. Wang, J. B. H. Tok and Z. Bao, Stretchable and self-healing polymers and devices for electronic skin, *Prog. Polym. Sci.*, 2013, **38**, 1961–1977.

8 D. Y. Wu, S. Meure and D. Solomon, Self-healing polymeric materials: a review of recent developments, *Prog. Polym. Sci.*, 2008, **33**, 479–522.

This journal is © the Owner Societies 2019

Phys. Chem. Chem. Phys., 2019, **21**, 10171–10184 | **10183**

9   T. C. B. McLeish, Tube theory of entangled polymer dynamics, *Adv. Phys.*, 2002, **51**, 1379–1527.

10 M. van Gurp and J. Palmen, Time–temperature superposition for polymeric blends, *J. Rheol.*, 1998, **65**, 5–8.

11 R. K. Bose, N. Hohlbein, S. J. Garcia, A. M. Schmidt and S. Van Der Zwaag, Connecting supramolecular bond lifetime and network mobility for scratch healing in poly(butyl acrylate) ionomers containing sodium, zinc and cobalt, *Phys. Chem. Chem. Phys.*, 2015, **17**, 1697–1704.

12 R. K. Bose, N. Hohlbein, S. J. Garcia, A. M. Schmidt and S. Van Der Zwaag, Relationship between the network dynamics, supramolecular relaxation time and healing kinetics of cobalt poly(butyl acrylate) ionomers, *Polymer*, 2015, **69**, 228–232.

13 J. D. Ferry, *Viscoelastic properties of polymers*, Wiley, 1980.

14 J. M. Dealy, D. J. Read and R. G. Larson, *Structure and rheology of molten polymers*, Hanser, Munich, 2013.

15 K. M. Kirkwood, L. Gary Leal, D. Vlassopoulos, P. Driva and N. Hadjichristidis, Stress relaxation of comb polymers with short branches, *Macromolecules*, 2009, **42**, 9592–9608.

16 M. Kapnistos, D. Vlassopoulos, J. Roovers and L. G. Leal, Linear rheology of architecturally complex macromolecules: comb polymers with linear backbones, *Macromolecules*, 2005, **38**, 7852–7862.

17 S. Bode, M. Enke, R. K. Bose, F. H. Schacher, S. J. Garcia, S. van der Zwaag, M. D. Hager and U. S. Schubert, Correlation between scratch healing and rheological behavior for terpyridine complex based metallopolymers, *J. Mater. Chem. A*, 2015, **3**, 22145–22153.

18 A. Susa, R. K. Bose, A. M. Grande, S. Van Der Zwaag and S. J. Garcia, Effect of the Dianhydride/Branched Diamine Ratio on the Architecture and Room Temperature Healing Behavior of Polyetherimides, *ACS Appl. Mater. Interfaces*, 2016, **8**, 34068–34079.

19 A. Susa, J. Bijleveld, M. Hernandez Santana and S. J. Garcia, Understanding the Effect of the Dianhydride Structure on the Properties of Semiaromatic Polyimides Containing a Biobased Fatty Diamine, *ACS Sustainable Chem. Eng.*, 2018, **6**, 668–678.

20 J. Wu, L. H. Cai and D. A. Weitz, Tough Self-Healing Elastomers by Molecular Enforced Integration of Covalent and Reversible Networks, *Adv. Mater.*, 2017, **29**, 1–8.

21 B. J. Gold, C. H. Hövelmann, N. Lühmann, N. K. Székely, W. Pyckhout-Hintzen, A. Wischnewski and D. Richter, Importance of Compact Random Walks for the Rheology of Transient Networks, *ACS Macro Lett.*, 2017, **6**, 73–77.

22 L. Leibler, M. Rubinstein and R. H. Colby, Dynamics of Reversible Networks, *Macromolecules*, 1991, **24**, 4701–4707.

23 F. Herbst, D. Döhler, P. Michael and W. H. Binder, Self-healing polymers via supramolecular forces, *Macromol. Rapid Commun.*, 2013, **34**, 203–220.

24 M. Ahmadi, L. G. D. Hawke, H. Goldansaz and E. Van Ruymbeke, Dynamics of Entangled Linear Supramolecular Chains with Sticky Side Groups: Influence of Hindered Fluctuations, *Macromolecules*, 2015, **48**, 7300–7310.

25 A. Susa, A. Mordvinkin, K. Saalwächter, S. Van Der Zwaag and S. J. Garcia, Identifying the Role of Primary and Secondary Interactions on the Mechanical Properties and Healing of Densely Branched Polyimides, *Macromolecules*, 2018, **51**, 8333–8345.

26 Q. Chen, Z. Zhang and R. H. Colby, Viscoelasticity of entangled random polystyrene ionomers, *J. Rheol.*, 2016, **60**, 1031–1040.

27 M. J. Mateyisi, J. U. Sommer, K. K. Müller-Nedebock and G. Heinrich, Influence of weak reversible cross-linkers on entangled polymer melt dynamics, *J. Chem. Phys.*, 2018, **148**, 244901.

28 S. Ankiewicz, N. Orbey, H. Watanabe, H. Lentzakis and J. Dealy, On the use of continuous relaxation spectra to characterize model polymers, *J. Rheol.*, 2016, **60**, 1115–1120.

29 V. Yesilyurt, A. M. Ayoob, E. A. Appel, J. T. Borenstein, R. Langer and D. G. Anderson, Mixed Reversible Covalent Crosslink Kinetics Enable Precise, Hierarchical Mechanical Tuning of Hydrogel Networks, *Adv. Mater.*, 2017, **29**, 1–6.

30 B. Reck and H. Ringsdorf, Combined liquid-crystalline polymers: rigid rod and semiflexible main chain polyesters with lateral mesogenic groups, *Makromol. Chem., Rapid Commun.*, 1986, **7**, 389–396.

31 J. Honerkamp and J. Weese, A nonlinear regularization method for the calculation of relaxation spectra, *Rheol. Acta*, 1993, **32**, 65–73.

32 I. McDougall, N. Orbey and J. M. Dealy, Inferring meaningful relaxation spectra from experimental data, *J. Rheol.*, 2014, **58**, 779–797.

33 T. Roths, M. Marth, J. Weese and J. Honerkamp, A generalized regularization method for nonlinear ill-posed problems enhanced for nonlinear regularization terms, *Comput. Phys. Commun.*, 2001, 279–296.

34 M. Baumgaertel and H. H. Winter, *Determination of relaxation and retardation spectra from dynamical mechanical data*, 1989, vol. 28.

35 A. R. Davies and R. S. Anderssen, *Sampling localization in determining the relaxation spectrum*, 1997, vol. 73.

36 T. Aida, E. W. Meijer and S. I. Stupp, Functional supramolecular polymers, *Science*, 2012, **335**, 813–817.

37 R. K. Bose, N. Hohlbein, S. J. Garcia, A. M. Schmidt and S. van der Zwaag, Connecting supramolecular bond lifetime and network mobility for scratch healing in poly(butyl acrylate) ionomers containing sodium, zinc and cobalt, *Phys. Chem. Chem. Phys.*, 2015, **17**, 1697–1704.

38 R. P. Wool and K. M. O'Connor, A theory of crack healing in polymers, *J. Appl. Phys.*, 1981, **52**, 5953–5963.

39 Y. H. Kim and R. P. Wool, A Theory of Healing at a Polymer Polymer Interface, *Macromolecules*, 1983, **16**, 1115–1120.

40 A. M. Grande, S. J. Garcia and S. Van Der Zwaag, On the interfacial healing of a supramolecular elastomer, *Polymer*, 2015, **56**, 435–442.

41 Y. Yang and M. W. Urban, Self-healing polymeric materials, *Chem. Soc. Rev.*, 2013, **42**, 7446–7467.

10184 | *Phys. Chem. Chem. Phys.*, 2019, **21**, 10171–10184

This journal is © the Owner Societies 2019